PHOTOCATALYTIC REDUCTION OF HEXAVALENT CHROMIUM WITH NICKLE-DOPED ZINC OXIDE/POLYANILINE NANOCOMPOSITES AND SUNLIGHT

A thesis presented to the faculty of the Graduate School of Western Carolina University in partial fulfillment of the requirements for the degree of Masters of Science in Chemistry.

By

Jennifer Paige Coleman

Advisor: Dr. Channa De Silva
Associate Professor of Chemistry
Department of Chemistry & Physics

Committee Members: Dr. Jerry R. Miller, Geosciences & Natural Resources Department
Dr. Arthur L. Salido, Chemistry & Physics Department

April 2018

ACKNOWLEDGEMENTS

I'd like to thank my advisor, Dr. Channa DeSilva, for all the guidance and helpful input throughout this project. I'd also like to thank Dr. Jerry Miller and Dr. Arthur Salido for serving on my committee and providing insightful suggestions. I'd like to express gratitude to Dr. Brian Dinklelmyer and and Dr. William Kwochka for their contributions to the photocatalytic and polymer portion of this research. I'd like to thank Dr. Carmen Huffman, the graduate student advisor, for her guidance through the graduate program. I'd like to recognize and thank the Advanced Materials Research Laboratory at Clemson University for the microscopy images. Thank you to The Graduate School at Western Carolina University for the funding through the 2018 Summer Research Assistantship. A huge thanks for all the faculty and staff at WCU for entertaining all of my inquiries and curiosities. A huge thanks to my mother, Dawne, for consistantly supporting my endeavors through the years. I'd also like to extend gratitude to my sister Whitney, my niece Ainsley, and all of my friends for helping to keep me smiling throughout this journey.

TABLE OF CONTENTS

List of Tables iv
List of Figures v
List of Abbreviations vi
Abstract vii
CHAPTER ONE: INTRODUCTION 1
Background 1
Chromium 1
Sources of Chromium in the Environment 2
Health Effects of Hexavalent Chromium 3
Traditional Cr Removal Methods 3
Project Design 4
Nanoscale Zinc Oxide Particles 4
Photocatalytic Reduction 5
Disadvantages of the Zinc Oxide Photocatalyst 6
Modifications to Improve the Zinc Oxide Photocatalyst 6
Previous Work 9
Goals 10
CHAPTER TWO: EXPERIMENTAL 12
Materials 12
Methods 12
Synthesis of the Catalyst 12
Characterization of Nanoparticle Composites 14
Photocatalysis 15
UV-Vis Quantitative Cr(VI) Analysis 17
CHAPTER THREE: RESULTS AND DISCUSSION 18
Synthesis 18
XRD Analysis 18
IR Analysis 19
DLS 21
TEM, SEM, and EDX Analysis 23
Photocatalytic Reduction 27
Reaction Mechanism 27
Reaction Mechanism of the Hole Scavenger 29
Optimization of Hole Scavenger 30
UV-Vis Calibration 31
UV-Vis Colorimetric Determination of Cr(VI) in Photoreduced Solutions 32
CHAPTER FOUR: CONCLUSIONS AND FUTURE DIRECTIONS 35
REFERENCES 36

LIST OF TABLES

Table 1. Zinc oxide and Nickel- doped zinc oxide DLS data. 22
Table 2. Cr(VI) concentrations remaining in photocatalytic reduction solutions containing 10 ppm Cr(VI) with ZnO-PANI and Ni-ZnO-PANI nanocomposites..... 33

LIST OF FIGURES

Figure 1. The chemical structure of (A) chromium (III) oxide and (B) the hexavalent dichromate anion 2
Figure 2. A diagram of the photocatalytic reduction of Cr(VI) and oxidation of H_2O by ZnO 5
Figure 3. Structure of cetyltrimethylammonium bromide (CTAB) 7
Figure 4. Structure of polyaniline 7
Figure 5. Zinc oxide-polyaniline heterojunction diagram 8
Figure 6. Reaction scheme for the synthesis of polyaniline 14
Figure 7. The oxidation of 1,5-diphenylcarbazide by hexavalent chromium produces reduced trivalent chromium and 1,5-diphenylcarbazone 15
Figure 8. XRD spectrum and Miller indices of ZnO and Ni-ZnO nanoparticles 18
Figure 9. The XRD spectra of (a) zinc oxide-polyaniline and (b) nickel-doped zinc oxide-polyaniline nanocomposites 19
Figure 10. The IR spectra of (a) zinc oxide and (b) nickel-doped zinc oxide nanoparticles 20
Figure 11. IR spectrum of polyaniline 20
Figure 12. The IR spectra of (a) polyaniline/zinc oxide and (b) polyaniline/nickel-doped zinc oxide nanocomposites 21
Figure 13. Stacked IR spectrum of ZnO, Ni-ZnO, PANI, ZnO-PANI, and Ni-ZnO-PANI 22
Figure 14. The TEM images of (a) and (b) nickel-doped zinc oxide nanoparticles 24
Figure 15. The TEM images of (a) and (b) nickel-doped zinc oxide polyaniline nanocomposites 24
Figure 16. The particle size distribution of Ni-ZnO nanoparticles 25
Figure 17. Particle size distribution of Ni-ZnO-PANI nanoparticles 25
Figure 18. SEM Image of nickel-doped zinc oxide nanoparticles 26
Figure 19. EDX spectra of nickel-doped zinc oxide nanoparticles 27
Figure 20. The Cr(VI) concentration in ppm after 120 minutes of sunlight exposure with varying volumes of the methanol hole scavenger 30
Figure 21. The calibration curve for Cr(VI) concentrations determined by the 1,5-DPC colorimetric UV-Vis method 31
Figure 22. The concentration of Cr(VI) during photocatalytic reduction with ZnO-PANI and Ni-ZnO-PANI nanocomposites 33
Figure 23. The removal percentage of Cr(VI) from a 10 ppm solution with ZnO-PANI and Ni-ZnO-PANI photocatalysts 34

LIST OF ABBREVIATIONS

α	alpha
$\mathring{A}$	angstrom or 10^{-10} meters
$^{\circ}$ C	degrees Celcius
λ	lamba; wavelength
μ	micro
π	pi
θ	theta
1,5-DPC	1,5-diphenylcarbazide
cm^{-1}	inverse centimeters
Cr(VI)	Hexavalent chromium
Cr(III)	Trivalent chromium
CTAB	cetyltrimethylammonium bromide
e^{-}	electron
eV	electron volts
EPA	The United States Environmental Protection Agency
g	grams
h^{+}	positively charged hole
FTIR	Fourtier-transform infrared
M	molar
meV	millielectron volts
mg	milligrams
mL	milliliters
mM	millimolar
mmol	millimoles
Ni-ZnO	nickel-doped zinc oxide nanoparticles
nm	nanometers
ppb	parts per billion
ppm	parts per million
PANI	polyaniline
RPM	rotations per minute
UV-Vis	ultraviolet-visible
V	volts
W	watts
XRD	X-ray diffraction
Nd-YAG	Neodymium-doped Yttrium Aluminum Garnet
ZnO	zinc oxide

ABSTRACT

PHOTOCATALYTIC REDUCTION OF HEXAVALENT CHROMIUM WITH NICKEL-DOPED ZINC OXIDE- POLYANILINE NANOCOMPOSITES AND SUNLIGHT

Jennifer Paige Coleman, Masters of Science in Chemistry

Western Carolina University (April 2019)

Advisor: Dr. Channa De Silva

The removal of hexavalent chromium (Cr(VI)) from aquatic systems is critical due to the extreme toxicity and high mobility of the contaminant in the environment. Semiconducting zinc oxide nanoparticles synthesized with a conducting polymer, such as polyaniline, have shown a high efficiency for the photocatalytic reduction of Cr(VI) to the less toxic form using visible light. Doping zinc oxide with nickel ions has also been shown to increase the photocatalytic efficiency of zinc oxide. I have synthesized zinc oxide-polyaniline and nickel-doped zinc oxide-polyaniline nanoparticles via microwave synthesis to determine the effect of nickel-doping on the photocatalytic reduction potential of the zinc oxide-polyaniline particles. XRD, FTIR, TEM, SEM, EDX and DLS measurements have confirmed the synthesis of zinc oxide and nickel-doped zinc oxide nanocrystals. The polymerization of the nanoparticles with polyaniline was confirmed with FTIR and TEM. Photocatalytic reduction experiments with hexavalent chromium (Cr(VI)) and a methanol hole scavenger were performed under an Atlas sunlight simulator. The remaining Cr(VI) concentrations were determined using the standard 1,5-diphenyl carbazide colorimetric method and UV-Vis spectroscopy. The Ni-ZnO-PANI nanocomposites showed a similar Cr(VI) removal efficiency to ZnO-PANI at 97.7% and 98.0%, respectively. The Ni-ZnO-PANI reduced about 5% more Cr(VI) in the first 90 minutes of sunlight exposure. Overall, there was not a significant difference between the Cr(VI) reduction efficiency of the ZnO-PANI and Ni-ZnO-PANI photocatalysts.

CHAPTER ONE: INTRODUCTION

Hexavalent chromium (Cr(VI)) is considered a priority pollutant that poses a threat to humans by the United States Environmental Protection Agency, due to the high solubility, mobility, and toxicity of Cr(VI) compounds in the environment.[1–3] The World Health Organization has classified Cr(VI) as a Group 1 carcinogen and in 2003, set a 50 ppb threshold limit for drinking water.[4,5] California set a more aggressive Public Health Goal of 0.020 ppb and maintains a maximum Cr(VI) level of 10 ppb for drinking water.[4,6] The development of remedial technologies is vital to achieving the threshold limits of this toxic pollutant.

Background

Chromium

Chromium exists in the environment as trivalent (Cr(III)) and hexavalent Cr(VI) compounds or ions, depending on the oxidation state of the metal.[4,6–10] Cr(III) is the less toxic of the two species and is an essential trace nutrient in animals.[5,6] In natural waters with a slightly acidic to neutral pH range, Cr(III) exists as Cr^{+3}, $Cr(OH)^{+2}$, and $Cr(OH)_2^{+}$ cations, chromium (III) oxide (see Figure 1), chromium hydroxide, or the $Cr(OH)_4^{-}$ anion.[8] These compounds tend to have a strong electrostatic attraction with amines and adsorb to sediment and clay particles, which removes the ions from solution by promoting precipitation and decreasing the potential mobility of the metal.[8]

Cr(VI) is chromium in its most oxidized form (6+) and is highly toxic.[6,9] Compounds containing Cr(VI) have a higher solubility than Cr(III) compounds and are readily transported through the environment in aqueous solutions, often contaminating surface and groundwater miles away from the point source of contamination.[10] Several Cr(VI) compounds exist in aqueous solutions and their speciation depends heavily on the pH of the system.[4,6,9,10] Dichromate ($Cr_2O_7^{2-}$) is the predominate anion in highly acidic solutions, whereas hydrogen chromate ($HCrO_4^{2-}$) and

chromate (CrO_4^{2-}) ions are dominate in waters in a basic or neutral pH range.[6,9,10] The chemical structures of trivalent chromium oxide and the hexavalent dichromate anion are shown in Figure 1 A & B, respectively.

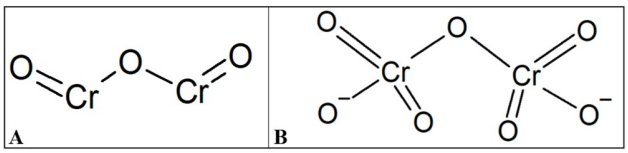

Figure 1. The chemical structure of (A) chromium (III) oxide and (B) the hexavalent dichromate anion

Sources of Chromium in the Environment

Chromium within the earth's crust is predominately found in chromite or chrome-iron ores associated with ultramafic rock formations.[4,8,11] The crustal average of Cr is around 122 ppm, with a range of 11 - 22 ppm Cr in soils.[8] Most of the naturally occuring Cr exists in a +3 oxidation state. However, Cr(III) can be oxidized to Cr(VI) by biological or other natural processes when the environment's pH, organic content, and eH (oxidation-reduction potential) are favorable for oxidation.[4,6,9,10] Soils or sediments containing manganese hydroxides and oxides have the potential to convert Cr(III) to Cr(VI).[4,9] The chlorination of water can also affect the speciation of aqueous chromium, often increasing Cr(VI) concentrations.[6]

Although some hexavalent chromium originates from natural sources, the majority of Cr(VI) pollution can be traced back to industrial processes.[8,10,12] Anthropogenic sources of hexavalent chromium contamination include electroplating, tanning/leather processing, mining, and metal finishing industries.[10,12,13] Cr(VI) contamination is also associated with some dye productions, wood preservation, refractories and smelting operations, and the improper disposal of mined chromite ore.[6,8,10,11] The accidental and intentional release of Cr(VI) compounds into the envi-

ronment from these industries has resulted in hundreds of Superfund sites listing Cr(VI) as a pollutant.[6]

Health Effects of Hexavalent Chromium

Hexavalent chromium is highly toxic, even in very small quantities.[6] The chromate anion can easily diffuse into cell membranes through sulfate channels, due to their similar tetrahedral structures.[5,6,9,12] Cr(VI) can be metabolized in humans by various pathways that produce Cr(V), and sulfur- and carbon-based radicals, which can produce hydroxyl radicals in Fenton-types reactions.[6] The hydroxyl radicals and Cr(V) cause the most oxidative stress on biomolecules and lead to various forms of cancer.[5,6,9,12] This internal oxidation has caused stomach, intestinal, lung, mouth, and liver cancer.[5,6,8,14]

Cr(VI) is classified as a DNA mutagen and causes DNA damage by binding to several amino acids and inhibiting the replication mechanism.[6] It silences the transcription of tumor supressing genes, resulting in tumors in the mouth, lungs, and stomach.[6] It is corrosive to the respiratory tract and can cause eye, nose, and throat irritation when inhaled.[6,8,14] Cr(VI) exposure has been shown to cause chronic ulcers and dermatitis.[8,14] Cr(VI) is acutely toxic through all possible exposure pathways and is extremely toxic to aquatic ecosystems.[6,8] Therefore, the prevention of environmental Cr(VI) release is critical to ensure the protection of human and ecological health.

Traditional Cr Removal Methods

Traditional methods for removing Cr(VI) from drinking water or waste effluent include liquid-liquid extraction, solid phase extraction, chemical reduction, and photocatalytic reduction.[9] Ionic liquid bases containing long chain tertiary amines are used as the organic solvent to remove dichromate anions during liquid-liquid extraction.[9] However, the amount of Cr-contaminated liquid waste is hazardous and expensive to dispose of. Solid-phase extraction methods employ an organic or inorganic stationary phase to physically remove Cr from the solution via adsorption or ion exchange processes.[9] Ion exchange resins have been used to adsorb metal pollutants, such as chromium and lead.[15] However, the ion exchange process often requires a range of aqueous and

organic solvents, which increases the waste disposal costs.[9] Inorganic stationary phases, such as silica, alumina, and clay minerals have been sucessful in removing Cr(VI) from aqueous solutions, but a further treatment is needed to induce desorption of the toxic Cr(VI) from the adsorbant, reduce it to Cr(III), and precipitate it out of solution.[9]

Project Design

Nanoscale Zinc Oxide Particles

Nanoparticles have been increasingly utilized for the remediation of contaminated water. Their high surface area to volume ratio increases the number of reaction sites on the particle's surface, therefore increasing the efficiency of toxin removal when compared to the bulk material.[16–18] Zinc oxide (ZnO) nanoparticles are increasingly being used for water treatment applications because they are relatively non-toxic, inexpensive, easily synthesized, and have a high redox potential.[16,19–21] ZnO nanoparticles have also been used for optic, electronic, sensor, electrode, nanolaser, and biomedical applications.[22,23]

ZnO nanoparticles can be synthesized via several methods, including thermal evaporation, chemical vapor deposition, template-based crystalization, and 'wet' solution based approaches.[23] The morphology of the ZnO nanoparticles can be manipulated by varying the starting reagents and synthetic parameters. The size and shape of the nanoparticles influence the optical and electronic properties of ZnO.[16,22,24] Some commonly documented ZnO particle shapes are the spherical, rod-like, flower, spindle, ribbon-like, hexagonal plate, and ponpom crystal arrangements.[21,25–27] Microwave-assisted synthesis of ZnO nanoparticles has become increasingly popular partially due to the wide range of ZnO morphologies that can be acheived by slightly altering microwave parameters, such as the power and reaction time.[21,26–28] Microwave synthesis is also adventageous in that the radiation provides homogenous heating of the reaction solution and significantly reduces the reaction time, while decreasing the energy input required for synthesis.[26,27]

Since ZnO is an n-type semiconductor, or material in which electrons can flow freely under

certain conditions based on the band gap of the material, it is capable of facilitating oxidation and reduction reactions.[17] ZnO has a high band gap of 3.37 eV and absorbs radiation below 380 nm, which falls in the ultra-violet (UV) region of the electromagnetic spectrum.[7,17,19,21–23,26,29,30] Therefore, ZnO is not photochemically active under visible light. However, ZnO exposure to UV radiation induces the promotion of electrons that can then be consumed in the reduction of another compound, in a process known as photocatalytic reduction.[7,29–31]

Photocatalytic Reduction

Photocatalytic reduction can occur when a semiconductor, such as ZnO, absorbs a photon of light with an energy that is equal to or greater than the band gap.[7,29,31] The absorbed photon promotes an electron from the semiconductor′s valance band to the conduction band, a higher energy unoccupied orbital.[20,21,29] The promotion of the electron leaves behind a positively charged 'hole' (h^+) in valance band,[7,21,31] as shown in Figure 2. The promoted electrons (e^-) and hole vacan-

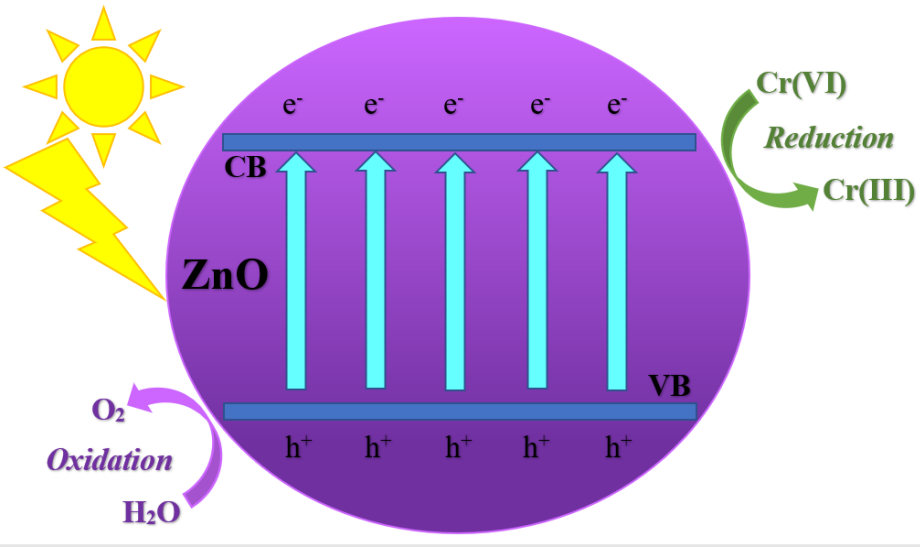

Figure 2. A diagram of the photocatalytic reduction of Cr(VI) and oxidation of H_2O by ZnO

cies can catalyze oxidation reduction reactions, including the reduction of hexavalent to trivalent

chromium, given that the electrons do not recombine with the holes through electrostatic attraction.[20,29] Hole scavengers, such as methanol and propanol, are added to the reaction solution to donate electrons, or consume the h^+'s, in the valence band of the photocatalyst.[32,33]

Disadvantages of the Zinc Oxide Photocatalyst

Although ZnO nanoparticles are a viable and commonly employed material for the photocatalytic reduction of contaminated water, there are several disadvantages associated with using ZnO for photocatalytic waste water treatment. ZnO particles are only stable within a 5-10 pH range and will dissolve in extremely acidic or basic solutions.[7] Synthesized ZnO particles typically have a poor monodispersity, without the addition of a surfactant, such as cetyltrimethylammonium bromide (CTAB).[17,21,22,34] They are susceptible to photodegradation over time and have a rapid e^-/h^+ recombination rate.[29] In order to decrease the photodegradation and increase the e^-/h^+ separation, ZnO particles have been combined with other materials to increase the efficiency and photostability.[29]

Modifications to Improve the Zinc Oxide Photocatalyst

CTAB Surfactant

Surfactants are often used in nanoparticle synthesis to control the particle size and diameter range.[22,34,35] Polyethylene glycol, ethylene glycol, sodium dodecyl sulfate, and CTAB have all been utilized as surfactants in ZnO synthetic procedures.[22,34–38] The CTAB surfactant used in this research is superior to the aforementioned surfactants because it contains a cationic ammonium functional group, which has a high affinity for Cr(VI) anions.[17,30,34] The chemical structure of CTAB is shown in Figure 3. CTAB reduces the surface tension of the reaction mixture and allows for a more homogeneous dispersion of the reactants.[22,34] The CTAB ionizes into CTA^+ and Br^- and forms an ion pair through a strong electrostatic attraction with the $Zn(OH)_4^{2-}$ intermediate in the ZnO synthesis.[30] It also controls the extent of particle growth by capping the ZnO particles and inhibiting particle agglomeration, resulting in monodispersed particles with a smaller average

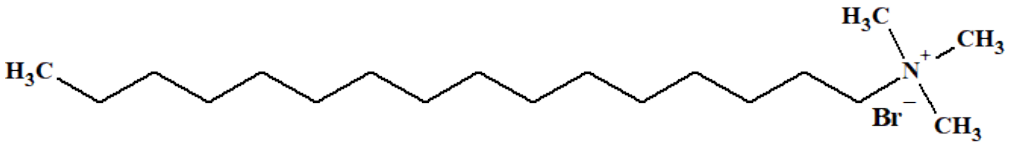

Figure 3. Structure of cetyltrimethylammonium bromide (CTAB)

diameter.[17,35] Since CTAB is photochemically active in visible light, it increases the photocatalytic activity of the ZnO by increasing the e^{-}/h^{+} separation.[34]

Polyaniline

Polyaniline (PANI) is a conducting polymer that has been extensively used to increase the photostability and photocatalytic efficiency of ZnO for water remediation.[21,32,39] It has been shown to be non-toxic in several toxicity studies.[40,41] PANI is not soluble in aqueous solvents and does not get absorbed into living organisms without the assistance of a copolymer, such as polyvinylpyrrolidone.[41] Although there is little interaction with biomolecules, the protonated amine group of PANI has a strong coulombic attraction towards Cr(VI) containing anionic ions.[9] PANI is a p-type semiconductor with a highly conjugated pi (π) electron system, which is illustrated in Figure 4.

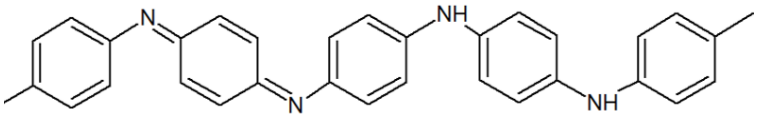

Figure 4. Structure of polyaniline

The high mobility of charge carriers within polyaniline's conjugated π system makes it an efficient electron donor and hole transporter.[32] PANI has a narrow band gap of 2.8 eV, which absorbs radiation in the visible region.[21,32,39] Since the band gap of PANI falls within the vis-

ible region (ZnO′s band gap is in the ultraviolet region), polymerizing PANI on the surface of ZnO nanoparticles increases the photocatalytic reduction potential of the system by increasing the range of radiation that will catalyze the electron excitation.[32] The efficiency of the system is improved because the electrons in the conduction band of PANI are transferred to the conduction band of ZnO, increasing the numbers of electrons available for reduction reactions.[21] Figure 5 depicts the charge transfer cycle across the ZnO-PANI heterojunction.

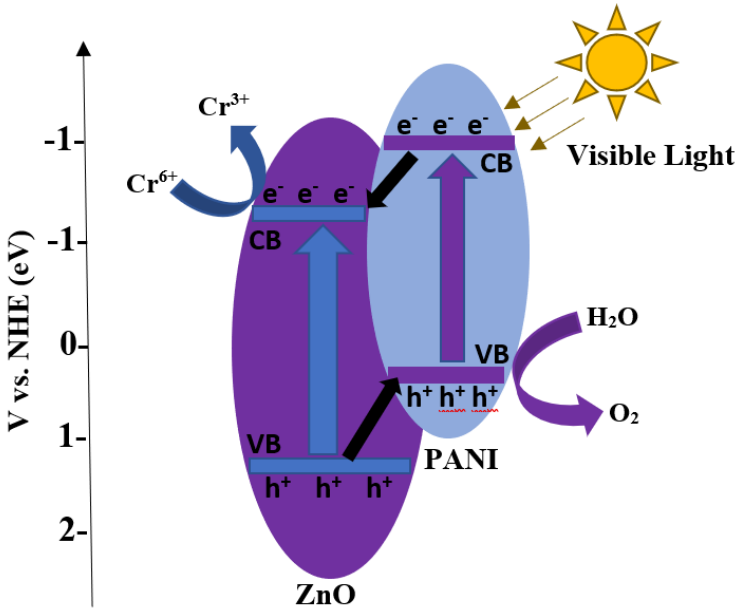

PCR.png

Figure 5. Zinc oxide-polyaniline heterojunction diagram

Nickel Doping

ZnO photocatalysts have also been doped with other transition metals, such as Fe, Ti, Ni, Co, Cu, Mg, and Ag, to improve the efficiency and photostability of the nanoparticles.[24,29,42,43] Divalent transition metals, such as Ni and Mg, are often doped into ZnO nanoparticles because they are isomorphic and easily substituted in to the ZnO hexagonal wurtzite crystal lattice.[24,32,44]

Turkyilmaz et. al. showed that nickel-doped ZnO had higher photocatalytic activity than manganese, iron, or silver-doped ZnO particles. Nickel is a p-type semiconductor that creates a p-n heterojunction when combined with ZnO.[32] This reduces the tendency for electron-hole recombination due to an induced internal electric field created by the p-n heterojunction.[29,32] Doping ZnO nanocrystals with Ni^{2+} ions reduces the band gap to 3.1 eV and allows for some visible light absorption.[29,32,37,43] Similar to PANI, the excited electrons in Ni′s conduction band are transferred to ZnO′s conduction band, which increases the available electrons for reduction of Cr(VI) ions.

Previous Work

Hasanpoor et. al. [26] used a microwave-assisted synthesis to produce both needle and flower shaped ZnO nanoparticles from $Zn(NO_3)_2$ and ammonia precursors. Adjusting the microwave parameters, such as the power and reaction time, changes the morphology and size of the ZnO nanoparticles.[26] Lui et. al. [28] developed a microwave-assisted synthesis of ZnO nanoparticles from zinc sulfate and sodium hydroxide for the photocatalytic reduction of Cr(VI). They varied the microwave reaction times (5-25 minutes) and found that the ZnO nanoparticles synthesized in 5 minutes had the highest (80%) Cr(VI) photoreduction efficiency for 250 minutes of UV exposure.[28]

Jin et. al. [20] synthesized ZnO nanoplates with a hydrothermal method using zinc acetate and urea precursors for the photocatalytic reduction of Cr(VI) under UV light. The standard 1,5-DPC colormetric method was used to determine the Cr(VI) photoreduction efficiency with UV-Vis spectroscopy.[20] The ZnO nanoplates exhibited a 55% photoreduction efficiency without the presence of a hole scavenger and an increased efficiency in the presence of phenol.[20] The hole scavenger consumes the photogenerated holes and phenol is oxidized to CO_2 and H_2O,[20] providing a synergist benefit of reducing Cr(VI) and degrading phenol, which is another common wastewater pollutant.[20] Qamar et. al. [31] synthesized ZnO nanoparticles with zinc nitrate and ammonium carbonate for a laser-assisted photocatalytic reduction of Cr^{6+}. They used methanol as

a hole scavnger and acheived a 95% removal efficiency using a high power Nd-YAG laser.[31]

Zou et. al. [21] polymerized ZnO nanoparticles from zinc chloride, sodium hydroxide and CTAB with PANI. The CTAB surfactant produced ZnO rod-like nanoparticles with a high monodispersity in the 100-200 nm range.[21] After polymerization with PANI, the ZnO-PANI particles showed a 92.7% removal efficiency of Cr(VI) upon visible light irradiation, compared to 0% photoreduction efficiency for pure ZnO.[21] Gunti et. al. used PANI to increase the stability and photocatalytic activity of graphene-doped ZnO nanoparticles. The polymerized nanowires degraded about 10% more methyl orange than the naked graphene-ZnO particles under visable light.[45]

Turkyilmaz et. al. [29] showed that nickel-doped ZnO had higher photocatalytic efficiency for the degradation of tartrazine than manganese, iron, or silver-doped ZnO particles. Singh et. al. analyzed Ni decorated ZnO and ZnO nanoparticles for their Cr(VI) reduction efficiency. They found the Ni-ZnO nanorods had a 98.7% reduction efficiency compared to a 10.3% reduction efficiency of pure ZnO.[14] Bhaumik et. al. [51] polymerized PANI on $Ni(OH)_2$ particles that showed a 99% Cr(VI) removal efficiency.

Given the increased efficiency of the previously reported modified ZnO photocatalysts, we decided to investigate the effect of creating an internal p-n junction within the ZnO nanoparticles by doping with nickel, in addition to a surficial polyaniline heterojunction, on the photocatalytic reduction potential of Cr(VI).

Goals

To the best of our knowledge, the effect of Ni-doping on the photocatalytic reduction potential of Cr(VI) by ZnO-PANI nanocomposites has not been previously reported. Our goal is to determine the effect that Ni-doping has on the ZnO-PANI system with respect to the efficiency of Cr(VI) photoreduction in aqueous solutions. Ni-ZnO and ZnO nanoparticles will be synthesized with a low temperature hydrothermal microwave-assisted method using the CTAB surfactant. A

polymer of aniline will be synthesized and polymerized onto the nanoparticles to increase the stability and photocatalytic potential under visible light by forming Ni-ZnO-PANI and ZnO-PANI composites. Methanol is used as a hole scavenger to further improve the reduction of Cr(VI) by the nanocomposites by donating electrons into the valence bands and consuming hydroxyl radicals. Photocatalytic reduction of Cr(VI) by ZnO-PANI and Ni-ZnO-PANI nanocomposites are analyzed using UV-Vis spectrometry and a 1,5-diphenylcarbazide colorimetric Cr(VI) detection method.

CHAPTER TWO: EXPERIMENTAL

Materials

Zinc nitrate hexahydrate ($Zn(NO_3)_2 \cdot 6\,H_2O$), sodium hydroxide (NaOH), nickel nitrate hexahydrate ($Ni(NO_3)_2 \cdot 6\,H_2O$), hydrochloric acid (HCl), tetrahydrofuran (THF), ammonium hydroxide (NH_4OH), potassium dichromate ($K_2Cr_2O_7$), trace metal grade nitric acid (HNO_3), methanol (CH_3OH), and 1-5 diphenylcarbazide (1,5-DPC) were purchased from Fisher Scientific. Aniline was obtained from J.T. Baker Chemical Company. Ammonium peroxisulfate (APS) and cetyltrimethylammonium bromide (CTAB) were purchased from Acros Organics. All reagents were used without further purification. All glasswear was acid washed with trace metal grade nitric acid. Ultrapure water (UP H_2O) with a resistivity of 18.2 $M\Omega$-cm was obtained from a Barnstead E-Pure system with a 0.2 μm hollow fiber filter.

Methods

Synthesis of the Catalyst

Synthesis of Zinc Oxide Nanoparticles

A solution of $Zn(NO_3)_2 \cdot 6\,H_2O$ (0.803 g, 2.70 mmol) and CTAB (0.109 g, 0.300 mmol) in UP H_2O (25 mL) was stirred for 20 minutes. A 20 mL solution of NaOH (0.159 g, 3.98 mmol) was added dropwise and stirred at room temperature for 1 hour. The solution was microwaved on a CEM Discover SP microwave synthesizer at 120 W for 30 minutes at 100° C. The microwave-assisted synthesis method is adventageous in that it shortens reaction times, requires less energy, and provides uniform heating to the reaction vessel. The solution was centrifuged at 5000 RPM for 45 minutes and rinsed 3x with UP H_2O. The nanoparticle precipitate was collected and dried at 60° C for 72 hours in a muffle furnace. The nanoparticles were stored in a freezer at 4° C until analysis and polymerization. The chemical equation of the above reaction is shown in Equation 1.

$$\mathrm{Zn(NO_3)_2 + NaOH \longleftrightarrow Zn(OH)_2 \xleftrightarrow{OH^-} Zn(OH)_4{}^{2-} + CTA^- + Br^- \longrightarrow} \quad (1)$$

$$\mathrm{(Zn(OH)_4){-}CTA_{\mathit{n}} + Br^- \xrightarrow[60^\circ\ C]{\Delta} \longrightarrow ZnO + H_2O + CTAB}$$

Synthesis of Nickel-doped Zinc Oxide Nanoparticles

A solution of $Zn(NO_3)_2 \cdot 6\,H_2O$ (0.803 g, 2.70 mmol) and $Ni(NO_3)_2 \cdot 6\,H_2O$ (0.0872 g, 0.300 mmol) in UP H_2O (25 mL) with CTAB (0.109 g, 0.300 mmol) was magnetically stirred for 20 minutes. A solution (20 mL) of NaOH (0.159 g, 3.98 mmol) was added dropwise and stirred at room temperature for 1 hour. The solution was microwaved at 120 W for 30 minutes at 100° C. The solution was centrifuged at 5000 RPM for 45 minutes and rinse with UP H_2O two times. The precipitate was collected and dried at 60° C for 72 hours in a muffle furnace.

Synthesis of Polyaniline

PANI was synthesized using a commonly reported method for aniline polymerization.[45–47] Briefly, a 10 mL of aniline and 100 mL of 1 M HCl were combined and stirred for 10 minutes in an ice bath. In a separate beaker, APS (1.25 g, 5.48 mmol) was dissolved in 100 mL of HCl (1 M) and added dropwise to the chilled aniline solution. The solution shifted from a light brown to a deep forest green color, indicating the formation of PANI. The solution was stirred in an ice bath for 4 hours and stirred overnight at room temperature to complete the polymerization. The polymer solution was poured into 200 mL of ultrapure water and stirred for five minutes. The dark green PANI was collected under vacuum filtration on a glass frit and rinsed with UP H_2O, 1 M HCl, and methanol until the filtrate was clear.

The collected precipitate was combined with 200 mL of NH_4OH (pH = 9) and stirred for

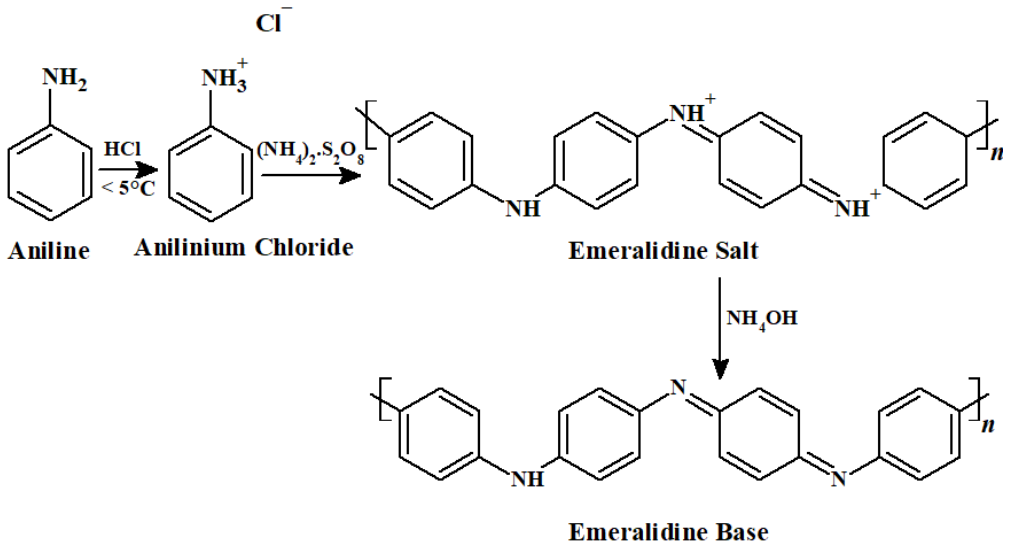

Figure 6. Reaction scheme for the synthesis of polyaniline

six hours to convert the polymer to the undoped emeraldine base form of PANI.[46] The reaction scheme for the synthesis is shown in Figure 6. The color change from green to dark blue is characteristic of the un-doped emeraldine base form of PANI.[45,46] The precipitate was collected on glass frit under vacuum filtration, rinsed with UP H_2O and methanol mixture (1:1) until the filtrate was clear to remove any unreacted oligomers, and dried on a vacuum overnight.

Polymerization of Nanoparticles

PANI was dispersed in THF (20 mL) and sonicated for 30 minutes. ZnO and Ni-ZnO nanoparticles were added to the polyaniline solution and stirred for 24 hours.[47] The weight ratio of nanoparticles to polyaniline was 2:1, or 2 mg of ZnO for every 1 mg of PANI.[45] The resulting ZnO-PANI and Ni-ZnO nanoparticles were collected by vacuum filtration on a glass frit and rinsed three times with ethanol before being dried at 55° C for 12 hours.

Characterization of Nanoparticle Composites

X-Ray Powder Diffraction (XRD) of the nanoparticles was performed on a desktop Mini-Flex+ XRD diffractometer from 15 - 75° 2θ with a scan speed of 0.5° per minute. The XRD data

were analyzed using Materials Data Jade 7 -software and the diffraction pattern was converted to Cu-Kα (λ =1.54059 $\AA$) for data analysis. The functional groups and structure were confirmed with a diamond tip Thermo iS10 FTIR Infrared (IR) Spectrometer. The size of the particles was determined from dynamic light scattering (DLS) on a Malvern Zetasizer Nano ZS dynamic light scattering instrument with a 632.8 nm Helium-Neon (He-Ne) laser source. DLS measurements were performed in UP H_2O with a ZnO refractive index of 1.99.

Photocatalysis

Quantitative Determination of Cr(VI) via UV-Vis Spectroscopy

The standard 1,5-diphenylcarbazide (1,5-DPC) colorimetric method was used to determine the concentration of Cr(VI) via UV-Vis absorption studies.[48] The 1,5-diphenylcarbazide molecule is oxidized to 1,5-diphenylcarbazone (1,5-DPCO) as Cr(VI) is reduced to Cr(III). The 1,5-DPCO complexes with the reduced Cr(III) to form a purple colored 1,5-DPCO(Cr(VI)) complex at a maximum absorbance of visible radiation at λ = 540 nm.[48,49] The reaction scheme is depicted below in Image 7.

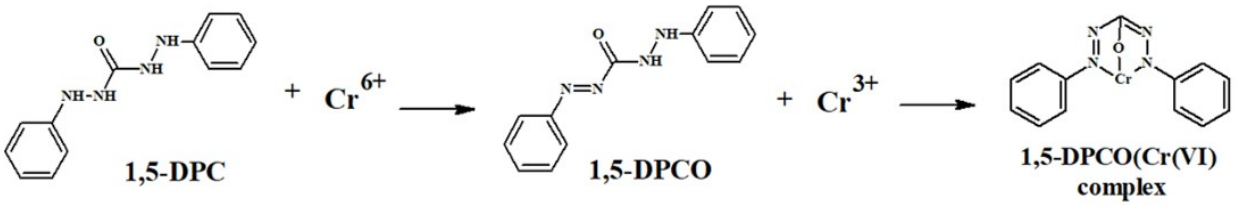

Figure 7. The oxidation of 1,5-diphenylcarbazide by hexavalent chromium produces reduced trivalent chromium and 1,5-diphenylcarbazone

The UV-Vis Spectrophotometer emits light in the ultraviolet/visible (UV/Vis) region and measures the radiation absorbed by a sample. The absorption of visible radiation induces electronic transitions in molecules.

Colormetric Reagent Preparation

A solution containing 1,5-diphenyl carbazide (1,5-DPC) (1.03 mmol, 250 mg) and acetone (50 mL) was mixed and stored in a brown glass bottle.[48] The 1,5-DPC solution was discarded once it became discolored.

Cr(VI) Calibration Standard Preparation

A 500 ppm stock solution of Cr(VI) was prepared by combining $K_2Cr_2O_7$ (141.1 mg, 0.482 mmol) and UP H_2O in a 100 mL volumetric flask.[8] A 5 ppm Cr(VI) standard solution was prepared by combining 1 mL of the Cr(VI) stock solution and 99 mL of UP H_2O in a 100 mL volumetric flask. A serial dilution of the Cr(VI) standard solution was used to create calibration standards ranging from 10 - 5000 ppb. To each 10 mL calibration solution, 0.400 mL of the 1,5-DPC solution, 0.490 mL of 0.1 M HNO_3, and 0.050 mL of methanol were added before diluting to 10 mL with UP H_2O.[8] The solutions were mixed and allowed to stand for 5 - 10 minutes for full color development before UV-Vis analysis.

Photocatalytic Reduction

The ZnO-PANI and Ni-ZnO-PANI photocatalysts were homogenized with a glass mortar and pestle. A 0.100 g portion of the photocatalyst was added to a 100 mL quartz round bottom flask. In a volumetric flask, 2 mL of the 500 ppm Cr(VI) stock solution was combined with 9 mL of 0.1 M HNO_3 and 5 mL of methanol and diluted with UP H_2O to 100 mL to create a 10 ppm Cr(VI) solution. The acidified 10 ppm (0.192 mM) Cr(VI) and methanol solution was added to the quartz round bottom with the photocatalyst and magnetically stirred in the dark for 30 minutes to reach the adsorption equilibrium. A 1.00 mL aliquot was extracted from the reaction solution, centrifuged to remove the photocatalyst, and analyzed for Cr(VI) concentration with the procedure described below.

An Atlas Suntest CPS+ sunlight simulator with a 300 W xenon bulb was used as a radiation source. Under continous stirring, the photolysis solution was exposed to the simulated sunlight

for 120 minutes, with a 1.5 mL aliquot extraction every 30 minutes. All aliquot extractions were centrifuged for 10 minutes to remove any suspended photocatalyst before further analysis.

UV-Vis Quantitative Cr(VI) Analysis

An Agilent Cary 5000 UV-Vis-NIR Ultraviolet-Visible-near Infrared Spectroscopy system in single beam mode was used for all UV-Vis analysis. All samples were analyzed from λ = 500 - 600 nm. However, only λ = 540 nm absorbances were used for concentration calculations, since it is the maximum absorbance wavelength of the 1,5-DPCO/Cr(VI) complex.[49] A solution of 0.400 mL 0.1 M HNO_3 and 0.400 mL of the 1,5-DPC and acetone solution were combined in a 10 mL volumetric flask and filled with UP H_2O. This mixture was allowed to sit for 5 - 10 mins before being transferred to a quartz cuvette and analyzed as a blank. The supernatent from the centrifuged samples were prepared in a similar manner, combining the extracted 1 mL of solution with the same volumes of H_2SO_4 and 1,5-DPC solution in 10 mL flasks. All solutions were mixed and allowed to sit for 5 - 10 mins for full color development before UV-Vis analysis.

CHAPTER THREE: RESULTS AND DISCUSSION

Synthesis

XRD Analysis

The X-ray diffraction spectra and Miller Indices of ZnO and Ni-ZnO nanoparticles are shown in Figure **??**. The diffraction peaks at angle 2θ of 31°, 34°, and 36° correspond to the (100), (002), and (101) Miller indices, respectively, and are consistent with the wurtzite hexagonal lattice structure of ZnO.[19,20,22,35] The lack of new peaks in the Ni-ZnO diffraction pattern indicates that the Ni^{2+} ions were incorporated into the ZnO crystal lattice rather than forming a unique crystal structure.[29,32] The XRD of the polymerized ZnO and Ni-ZnO nanoparticles produced similar

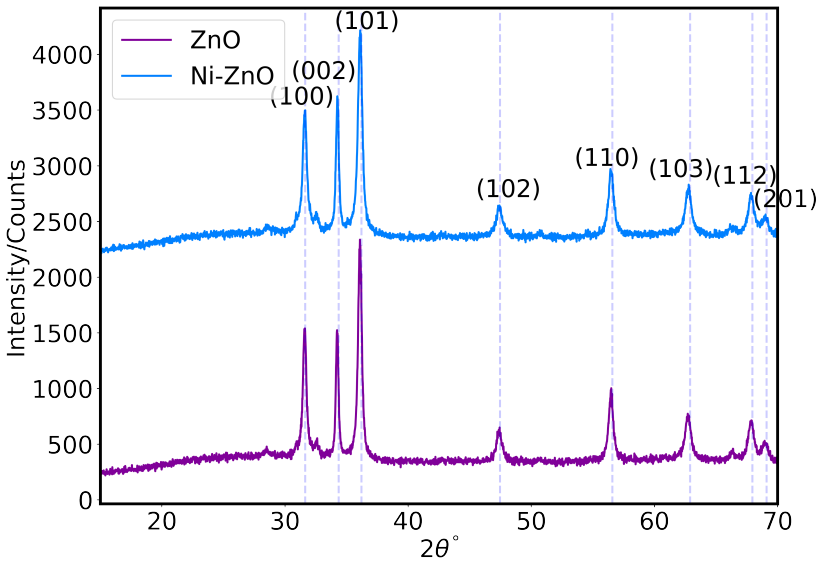

Figure 8. XRD spectrum and Miller indices of ZnO and Ni-ZnO nanoparticles

spectra and are shown in Figure 8. Polyaniline is amorphous (non-crystalline) and therefore does not diffract X-ray radiation or produce characteristic XRD peaks. The ZnO hexagonal wurtzite pattern that was obtained from the XRD analysis of the ZnO-PANI and Ni-ZnO-PANI nanocomposites and the dark blue PANI color of the sample confirm that the nanoparticles have adhered to the polymer during the polymerization technique, rather than being vaccummed out of the polymerization reaction solution.

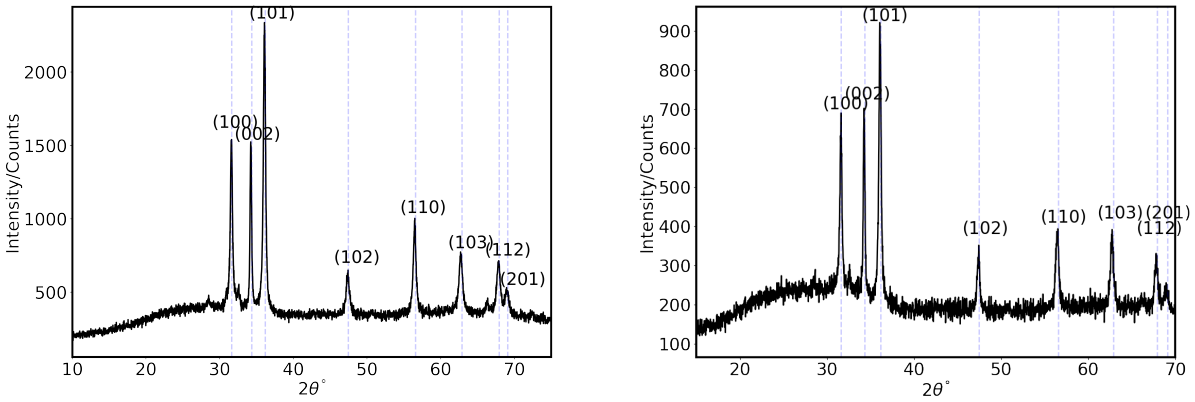

(a) ZnO-PANI (b) Ni-ZnO-PANI

Figure 9. The XRD spectra of (a) zinc oxide-polyaniline and (b) nickel-doped zinc oxide-polyaniline nanocomposites

IR Analysis

The IR spectra of the ZnO and Ni-ZnO nanoparticles are shown in Figure 10. The peak around 3385 cm^{-1} is the OH stretch of the hydrated ZnO.[16,50] The appearance of a new peak around 3490 cm^{-1} in Figure 10b is the Ni-OH stretch, which indicates the success of the Ni-doping process.[51] The ZnO stretch is shown by the peak around 500 cm^{-1}, which is evident in both the ZnO and Ni-ZnO samples.[16,50] There is a slight shift toward higher wavenumbers in the Ni-ZnO samples (Figure 10) which is consistent with previous reports.[51]

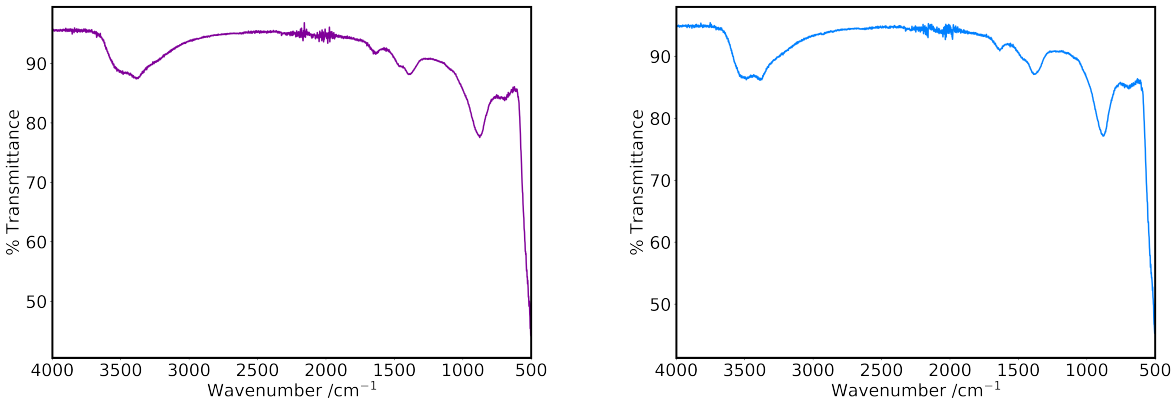

(a) ZnO (b) Ni-ZnO

Figure 10. The IR spectra of (a) zinc oxide and (b) nickel-doped zinc oxide nanoparticles

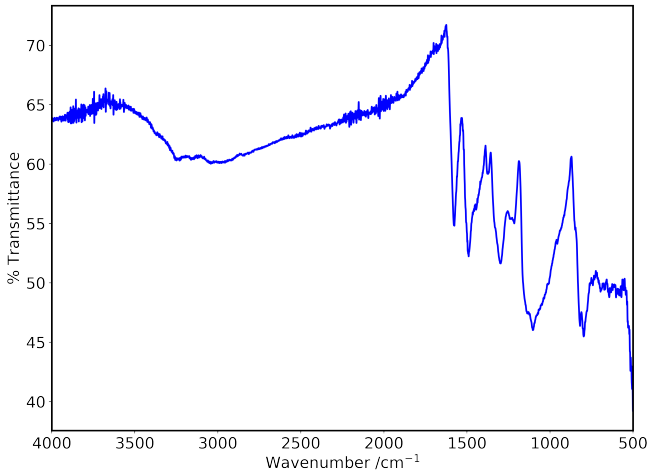

Figure 11. IR spectrum of polyaniline

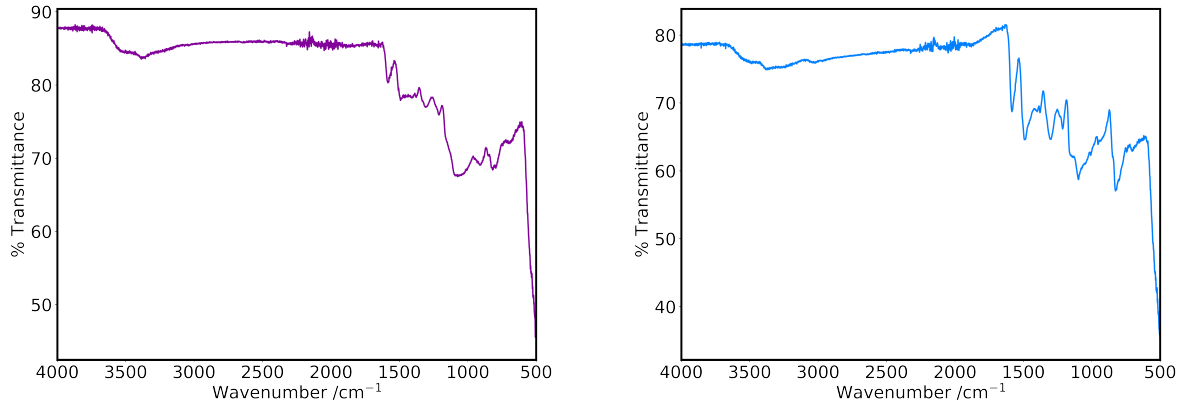

(a) PANI-ZnO (b) PANI-Ni-ZnO

Figure 12. The IR spectra of (a) polyaniline/zinc oxide and (b) polyaniline/nickel-doped zinc oxide nanocomposites

The IR spectrum of PANI is depicted in Figure 11. Two of the characteristic PANI IR peaks are around 1580 cm^{-1} and 1490 cm^{-1}, corresponding to the C=C stretching vibration of the quinzoid ring and benzoid ring, respectively.[39,45,50] The peaks at 1378 cm^{-1} and 1300 cm^{-1} are the C-N stretching vibration of the quinzoid ring and benzoid ring, respectively. The C-H stretching vibration produces the peak around 800 cm^{-1}.[16,39,45,50] The IR spectra of the (a) ZnO and (b) Ni-ZnO particles after polymerization with PANI are shown in Figure 12. The same characteristic PANI and ZnO / Ni-ZnO peaks that are discussed above are also evident in both spectra and is evident from the stacked spectrum in Figure 13.

DLS

Table 1 shows the average diameter (nm) and the polydispersity index (PDI) for the ZnO and Ni-ZnO nanoparticles. The PDI is an indicator of the size uniformity of the particles. PDI values range from 0-1, with 0 representing no variation in the size of the dispersed nanoparticles. The ZnO nanoparticles had an approximate average diameter of 275 nm with a PDI of 0.284, which indicates a small range of particle sizes in the sample. The average diameter of the Ni-ZnO par-

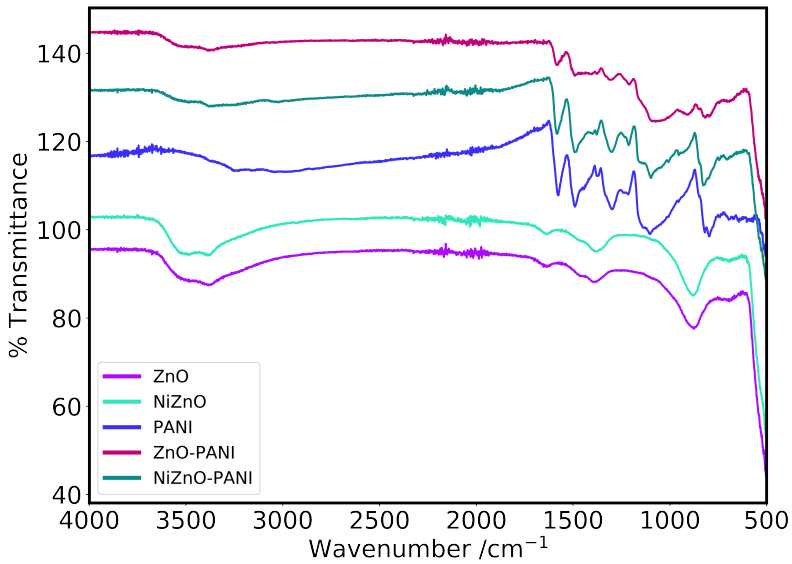

Figure 13. Stacked IR spectrum of ZnO, Ni-ZnO, PANI, ZnO-PANI, and Ni-ZnO-PANI

Table 1. Zinc oxide DLS data.

Trial	**Avg Dia.(nm)**	**PDI**
ZnO	275.1	0.284
Ni-ZnO	259.0	0.243

ticles was around 260 nm with a PDI of 0.243, which indicates more monodispersity within the sample. The smaller size of the Ni-doped particles is unexpected since the atomic radius of Ni at 0.69 $\AA$ is slightly larger than Zn at 0.60 $\AA$.[29,32] However, the reduction of particle size upon Ni-doping of ZnO particles has been documented.[24,32,43]

TEM, SEM, and EDX Analysis

The TEM images were obtained on a Hitachi H-9500 transmission electron microscope. The TEM images of the Ni-ZnO nanoparticles are shown in Figure 14 with a 100 nm scale (a) and a 50 nm scale (b). The Ni-ZnO nanoparticles range in size from around 20 nm to 200 nm and are aggregated into clusters. The dominant nanoparticle shapes are hexagonal and rectangular plate-like particles with some irregularly shaped particles.

Figure 15 shows the polymerized Ni-ZnO-PANI nanoparticles with a 100 nm scale (a) and a 50 nm scale (b). The process of polymerizing the nanoparticles degrades and eats away at the surface of the Ni-ZnO nanoparticles.[21] The Ni-ZnO nanoparticles in the 20-40 nm size range appear to have been eliminated during polymerization, while the largest nanoparticles have reduced in size from about 200 nm to about 140 nm. The majority of Ni-ZnO-PANI nanoparticles are rectangular in shape, although hexagonal and irregular nanoparticle shapes are still present.

The particle size distribution, determined from the TEM images, of the Ni-ZnO and Ni-ZnO-PANI nanoparticles is shown in Figures 16 and 17, respectively. The average diameter of the Ni-ZnO nanoparticles was around 60 nm. The polymerized Ni-ZnO-PANI nanoparticles had an average diameter of 80 nm. The increase in particle size can be attributed to the polymerization method of PANI in THF degrades the Ni-ZnO and destroys some of the smaller nanoparticles. This phenomena has been previously documented.[21]

The SEM images and EDX spectra were obtained on a Hitachi HD-2000 scanning electron microscope. The SEM image of the Ni-ZnO nanoparticles in Figure 18 shows the surface of the metal oxide. The surface of the agglomerated nanocrystals appears to be rough and angular. Surface defects in metal oxide photocatalysts have been shown to improve the photocatalytic

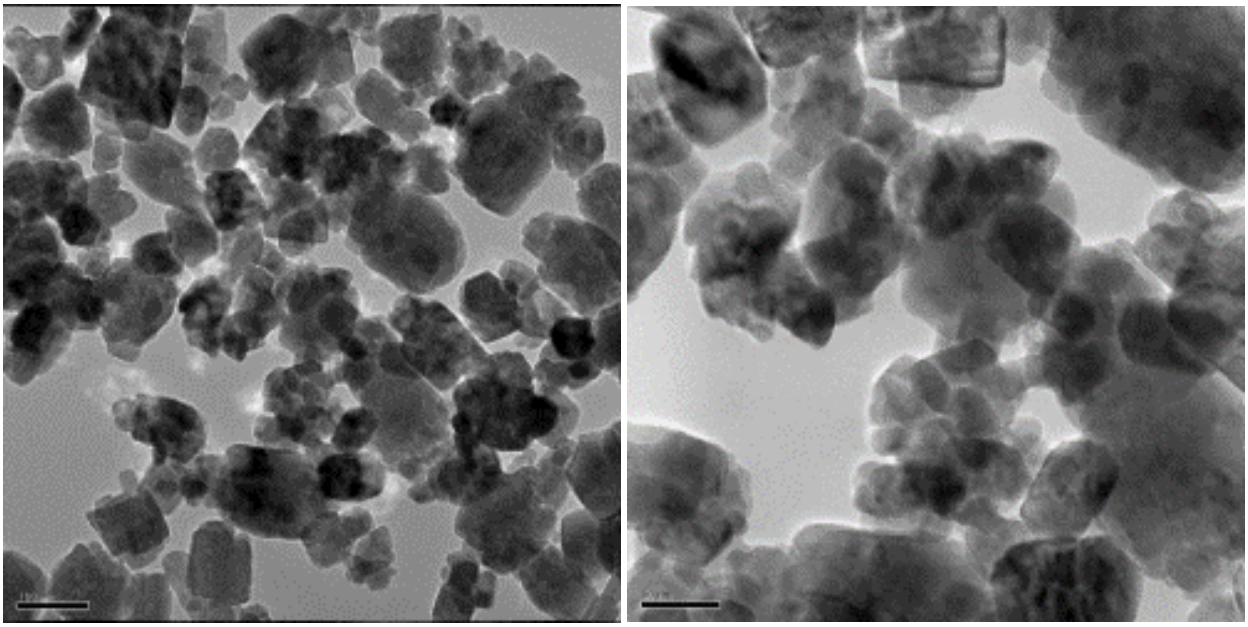

(a) Ni-ZnO: 100 nm scale (b) Ni-ZnO: 50 nm scale

Figure 14. The TEM images of (a) and (b) nickel-doped zinc oxide nanoparticles

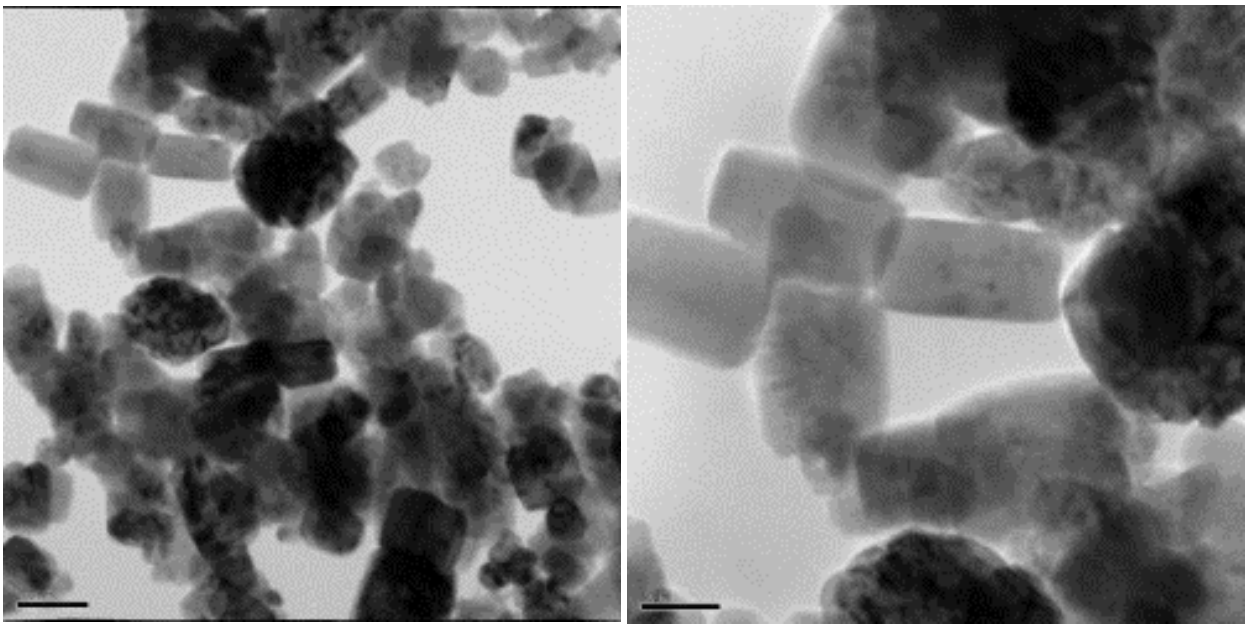

(a) Ni-ZnO-PANI: 100 nm scale (b) Ni-ZnO-PANI: 50 nm scale

Figure 15. The TEM images of (a) and (b) nickel-doped zinc oxide polyaniline nanocomposites

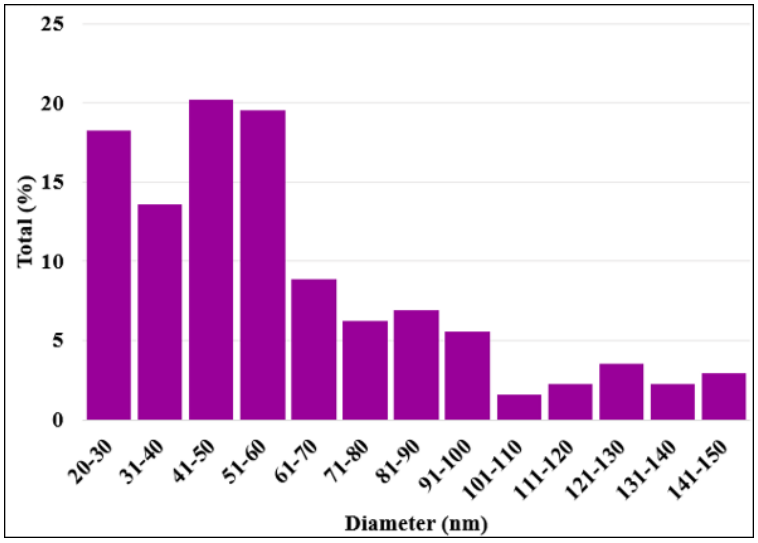

Figure 16. The particle size distribution of Ni-ZnO nanoparticles

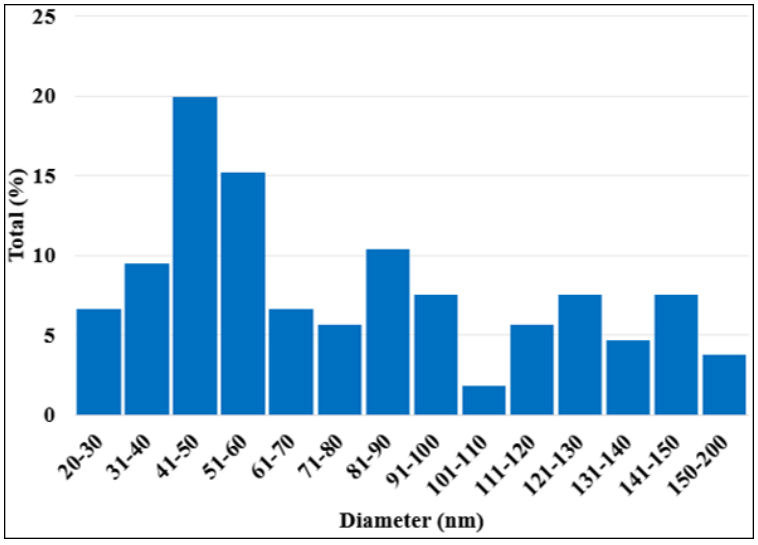

Figure 17. Particle size distribution of Ni-ZnO-PANI nanoparticles

reduction efficiency by trapping excited electrons and reducing the tendency for e^-/h$^+$ recombination.[34,42] The hexagonal and rectangular shape of the nanoparticles and relatively broad size range are also evident in the SEM image.

The energy dispersive X-ray (EDX) spectra, shown in Figure 19, gives an elemental analysis of the sample by measuring the energy (keV) of the X-rays released as excited electrons relax back to their ground state. The EDX confirms the presence of Zn, Ni, and O atoms in the sample. The relative heights of the 8.5-9 keV Zn peak and 8 keV Ni peak semi-quantitatively represent the ratio of Zn to Ni atoms, which appears close to the 10:1 desired Zn:Ni ratio.

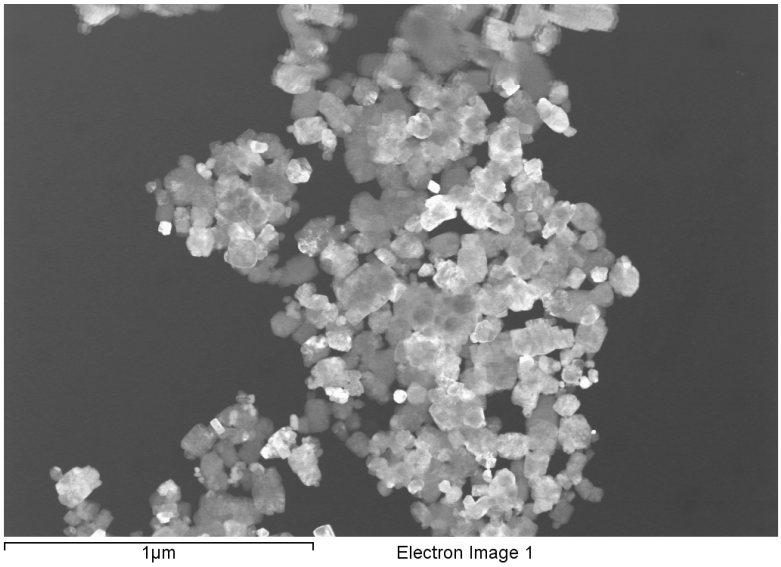

Figure 18. SEM Image of nickel-doped zinc oxide nanoparticles

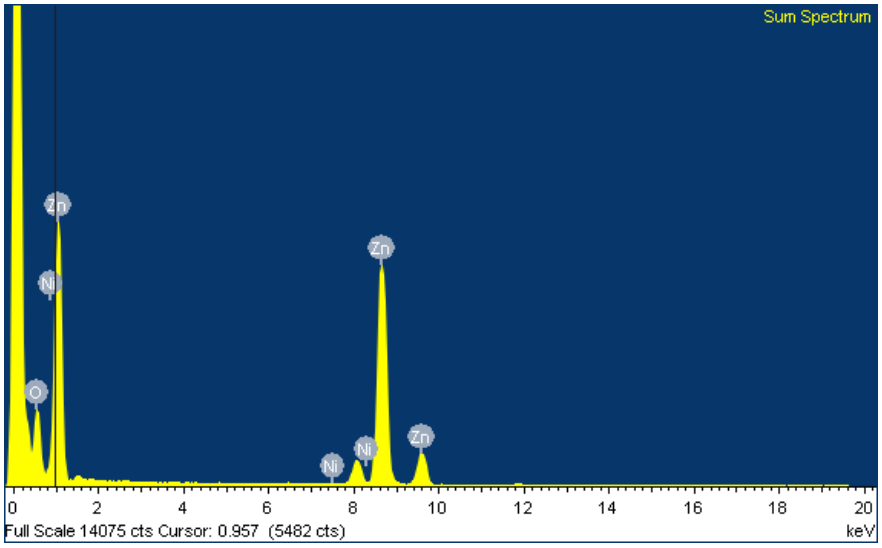

Figure 19. EDX spectra of nickel-doped zinc oxide nanoparticles

Photocatalytic Reduction

Reaction Mechanism

The reduction of the dichromate anion is a multi-electron process. Reactions 2 and 3 show the chemical equations of the reduction of dichromate ($Cr_2O_7{}^-{}_2$) in acidic and neutral conditions.[7,29,52,53]

$$Cr_2O_7{}^{-2} + 14\,H^+ + 6\,e^- \longrightarrow 2\,Cr^{+3} + 7\,H_2O \tag{2}$$

$$CrO_4{}^{-2} + 8\,H^+ + 3\,e^- \longrightarrow Cr^{+3} + 4\,H_2O \tag{3}$$

Since PANI is a conducting polymer, the excited e^- in PANI′s conducting band are transferred to the conducting band of ZnO or Ni-ZnO.[47] Simultaneously, the h^+ from the valence band of the metal oxide migrates to the valence band of PANI, which increases the e^- / h^+ separation and reduces electrostatic recombination.[47] The mechanism for the photocatalytic reduction of Cr(VI) anions by ZnO-PANI composites is a multi-step, radical dependent process that is

described below.[45,47] First, the photocatalyst is exposed to radiation to excite e^- and create the e^-/h^+ pair, as shown in Reaction 4.[53]

$$\mathrm{ZnO} + \mathrm{h}\nu \longrightarrow \mathrm{ZnO}(\mathrm{h}^+/e^-) \tag{4}$$

The e^- in the conducting bands can be directly consumed to reduce $Cr_2O_7^{2-}$ (Reaction 2). The excited e^- can react with dissolved oxygen (O_2) in the solution to form superoxide radicals ($O_2^{\cdot -}$) that donate e^- to and reduce Cr(VI) (Reaction 5).[45] The $O_2^{\cdot -}$ can also react with H_2O to form OH^- and $OOH^{\cdot}$ that further react to form hydrogen peroxide (H_2O_2) and hydroxyl radicals ($OH^{\cdot}$). These reactions are shown below in Reactions 6 and 7.

$$2\,e^- + \mathrm{O_2} \longrightarrow \mathrm{O_2}^{\cdot -} \tag{5}$$

$$\mathrm{O_2}^{\cdot -} + \mathrm{H_2O} \longrightarrow \mathrm{OOH}^{\cdot} + \mathrm{OH}^- \tag{6}$$

$$\mathrm{OOH}^{\cdot} + \mathrm{H_2O} \longrightarrow \mathrm{H_2O_2} + \mathrm{OH}^{\cdot} \tag{7}$$

$$\mathrm{O_2} + \mathrm{H}^+ + \mathrm{ZnO}(e^-) \longrightarrow 2\,\mathrm{H_2O_2} \tag{8}$$

The promoted e^- can also react with dissolved O_2 and H^+ to form H_2O_2 (Reaction 8). Cr(VI) reacts with H_2O_2 in acidic solution to form Cr(III), O_2, and H_2O (Reaction 9).[54]

$$\mathrm{Cr_2O_7}^{-2} + \mathrm{H_2O_2} + 8\,\mathrm{H}^+ \rightleftharpoons 2\,\mathrm{Cr}^{+3} + 2\,\mathrm{O_2} + 5\,\mathrm{H_2O} \tag{9}$$

The H_2O_2 is inherently unstable and can dissociate into two $OH^{\cdot}$ (Reaction 10).[55] Excited e^- can also react with H_2O_2 and produce OH^- and $OH^{\cdot}$ (Reaction 11).

$$H_2O_2 \longrightarrow OH^{\cdot} + OH^{\cdot} \tag{10}$$

$$H_2O_2 + e^- \longrightarrow OH^{\cdot} + OH^- \tag{11}$$

$$2\,OH^{\cdot} \longrightarrow H_2O_2 \tag{12}$$

Although two $OH^{\cdot}$ can react to reform H_2O_2 (Reaction 12), the $OH^{\cdot}$ is a strong oxidizer and can oxidize the photoreduced Cr(III) back to Cr(VI). Hydroxyl radicals are also produced when h^+ interacts with H_2O (Reaction 13) and in Reaction 7.

$$h^+ + H_2O \longrightarrow OH^{\cdot} + H^+ \tag{13}$$

Electron donating hole scavengers are often added to the reaction solution to counteract the production of the hydroxyl radicals.

Reaction Mechanism of the Hole Scavenger

Methanol (CH_3OH) was chosen as a hole scavenger. The CH_3OH scavenges the h^+ in the valence band to produce methanol radicals ($CH_2OH^{\cdot}$) (Reation 14). The hydrogen in the α position of the hydroxyl group of the hole scavenger is abstracted to form a radical.[33,56,57] The methanol radical is oxidized into formaldehyde and donates e^-'s to the valence band, as shown in Reaction 15.[31,55] The formaldehyde is further oxidized to formic acid before being converted to CO_2 and H_2O.[33]

$$CH_3OH + h^+ \longrightarrow CH_2OH^{\cdot} \tag{14}$$

$$CH_2OH^{\cdot} \longrightarrow CH_2O + H^+ + e^- \tag{15}$$

The $CH_2OH^{\cdot}$ has a negative oxidative potential (-0.74 V), allowing Reaction 15 to proceed and produce formaldehyde (CH_2O), H^+, and e^- to replace the positively charged vacencies in the valence band or to donate to the conducting band, reducing the rate of e^-/h^+ recombination.[55]

$$OH^{\cdot} + CH_3OH \longrightarrow CH_2OH^{\cdot} + H_2O \tag{16}$$

The use of a methanol hole scavenger does not directly consume the photogenerated holes, as Reactions 14 & 15 would suggest. Instead, the hydroxyl radicals react and radicalize CH_3OH (Reaction 16), which then produces e^- via Reaction 14.[55]

Optimization of Hole Scavenger

The most efficient volume of methanol hole scavenger was determined experimentally by photocatalytically reducing 10 mL of a 10 ppm Cr(VI) solution with different amounts methanol and selecting the volume ratio with the best reduction potential. (Figure 20). The 0.5 mL of methanol

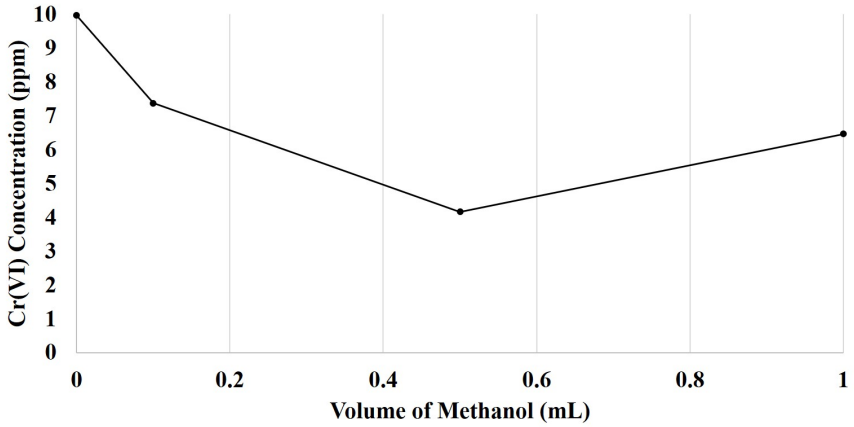

Figure 20. The Cr(VI) concentration in ppm after 120 minutes of sunlight exposure with varying volumes of the methanol hole scavenger

hole scavenger reduced the largest amount of Cr(VI) at 5.8 ppm. The 1 mL methanol solution

reduced 3.5 ppm, followed by the 0.1 mL methanol solution that only reduced 2.6 ppm during the 120 minute irradiation time. Therefore, a 1:20 volume ratio of acidified Cr(VI) solution to methanol was determined to be more efficient than the other volume ratios and was used for the remainder of the experiment. Chakrabarti et. al. used methanol as a hole scavenger with ZnO to reduce Cr(VI) and found the 1:20 ratio to be the optimal for photoreduction and removal efficiency.

UV-Vis Calibration

The UV-Vis calibration curve of 1,5-DPC-Cr complex at the maximum absorbance of 540 nm for varying concentrations of Cr(VI) in aqueous solution is shown in Figure 21. The line of best fit gives a linear equation of A = 36282*C + 0.0372 and an R^2 value of 0.9994. The y-intercept is not zero because the calibration curve becomes non-linear below 10 ppb, which is the limit of detection (LOD) for the 1,5-DPC colorimetric method.[8]

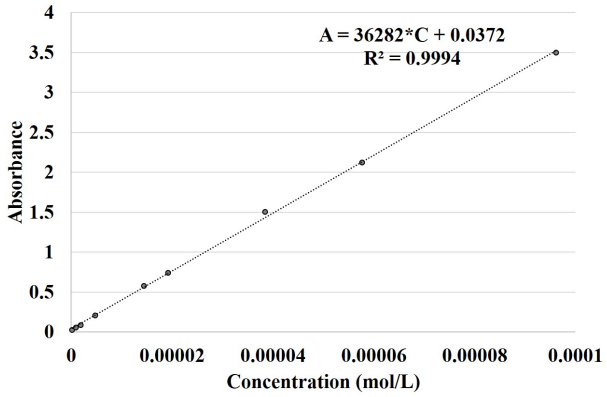

Figure 21. The calibration curve for Cr(VI) concentrations determined by the 1,5-DPC colorimetric UV-Vis method

UV-Vis Colorimetric Determination of Cr(VI) in Photoreduced Solutions

Beer's Law (Equation 17) was used to determine the Cr(VI) concentrations after photoreduction. The amount of light the sample absorbs at a certain wavelength is the absorbance (A). The molar absorptivity coefficient (ε) of the oxidized 1,5-DPCO-Cr complex was determined experimentally to be 36282 L mol^{-1} cm^{-1}, which is close to the previously reported 40,000 L mol^{-1} cm^{-1}.[8,48] The path length of the sample (b) was 1 cm.

$$A = \varepsilon b C \tag{17}$$

where, A is the absorbance, ε is the molar absorbance coefficient (L mol^{-1} cm^{-1}), b is the path length of the sample in cm, and C is the concentration in mol L^{-1}. The percentage of Cr(VI) that was removed from the photoreduced solutions was determined via Equation 18.

$$RemovalPercentage = \frac{C_0 - C_t}{C_0} * 100 \tag{18}$$

where, C_0 is the initial concentration and C_t is the time-dependent aliquot concentration. The calculated concentrations of Cr(VI) remaining at each analysis interval in the ZnO-PANI and Ni-ZnO-PANI photoreaction solution are shown in Table 2 and Figure 22. The time dependent removal percentages of Cr(VI) in the ZnO-PANI and Ni-ZnO-PANI photoreduced solutions are shown in Table 2 and Figure 23.

It is evident from Figures 22 and 23 that the Ni-ZnO-PANI reduced more Cr(VI) than the ZnO-PANI during the first 90 minutes. However, the ZnO-PANI reduced slightly more Cr(VI) (30 ppb) than Ni-ZnO-PANI in 120 minutes. Since the pH of the solution (1-2) was below the point of zero charge of ZnO (8.8-9.5), any unpolymerized ZnO surfaces are positively charged and the dichromate anion can be adsorbed to the ZnO surface.[7] The adsorption removal efficiency of Cr(VI) by the ZnO-PANI and Ni-ZnO-PANI nanocomposites is around 18%. Both the

Table 2. Cr(VI) concentrations remaining in photoreduced solutions containing 10 ppm Cr(VI) with ZnO-PANI and Ni-ZnO-PANI nanocomposites

	ZnO-PANI		Ni-ZnO-PANI	
Time (mins)	Conc. (ppm)	Removal (%)	Conc. (ppm)	Removal (%)
0- Initial	9.99	0	9.99	0
0- Adsorption	8.14	18.5	8.28	17.1
30	5.73	42.7	5.05	49.4
60	2.98	70.2	2.50	75.0
90	1.22	87.7	0.870	91.3
120	0.200	98.0	0.230	97.7

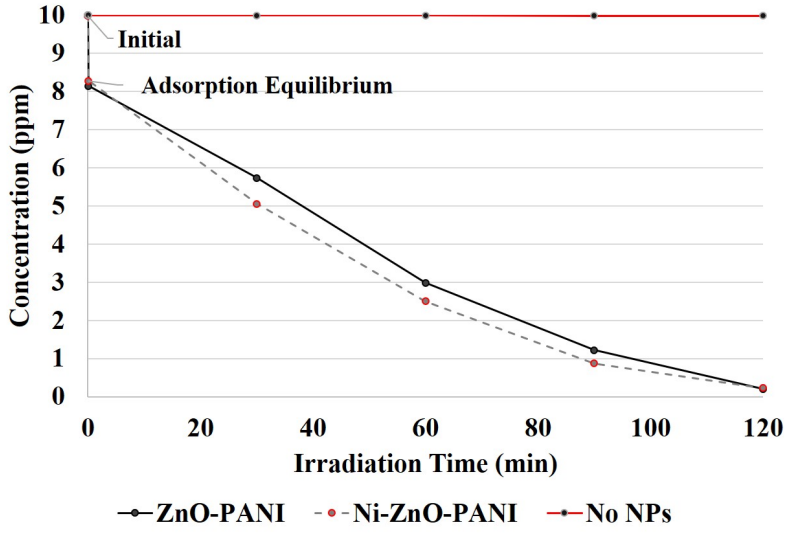

Figure 22. The concentration of Cr(VI) during photocatalytic reduction with ZnO-PANI and Ni-ZnO-PANI nanocomposites

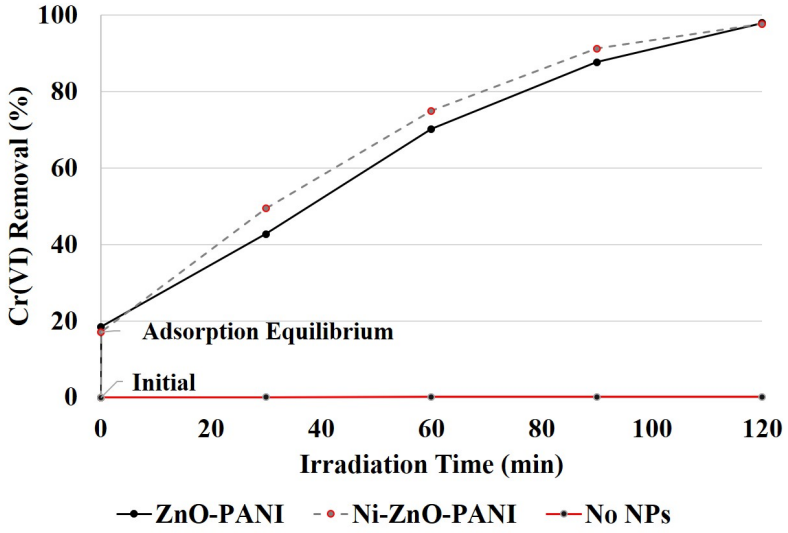

Figure 23. The removal percentage of Cr(VI) from a 10 ppm solution with ZnO-PANI and Ni-ZnO-PANI photocatalysts

ZnO-PANI and Ni-ZnO-PANI nanocomposites reduced about 98% of the 10 ppm Cr(VI) solution, which is higher than the 92.7% removal of ZnO-PANI nanoparticles synthesized by Zou et. al. There is unlikely an appreciable statistical difference in the ZnO-PANI and the Ni-ZnO-PANI photocatalyst's removal efficiency, although more trials would need to be performed to confirm this hypothesis. The solution with no photocatalyst showed minimal reduction (0.02 ppm total), which can be attributed to the adsorption and reduction of Cr(VI) into the surface of the quartz flask. The red line in Figures 22 and 23 represents the solution containing no nanoparticles (No NPs).

CHAPTER FOUR: CONCLUSIONS AND FUTURE DIRECTIONS

The synthesis of ZnO and Ni-doped ZnO nanoparticles via a microwave-assisted low temperature hydrothermal method and a CTAB surfactant produced irregular hexagonal and rectangular nanoparticles in the 20-150 nm size range. XRD analysis confirms the formation of the hexagonal wurtzite crystal structure in both the pure ZnO and Ni-doped ZnO nanoparticles. The IR spectra are also consistent with ZnO and Ni-ZnO nanocrystals. The polymerization of ZnO and Ni-ZnO nanocomposites was confirmed by XRD and IR analysis, and TEM images. The photocatalytic reduction of Cr(VI) with ZnO-PANI and Ni-ZnO-PANI nanocomposites under simulated sunlight respectively had a 98.0% and 97.7% removal efficiency. However, the Ni-ZnO-PANI had on average a 5% lower removal percentage for Cr(VI) during the first 90 minutes. More trials are needed to confirm the statistical significance of these results.

Future work should include optimizing the amount of nickel dopant to enhance the photocatalytic potential of the system. The doped particles should be dissolved and analyzed via inductively coupled plasma optical emission spectroscopy (ICP-OES) to confirm the concentration of Ni dopant. Varying ratios of PANI to Ni-ZnO nanoparticles should also be analyzed for effects on the photocatalytic reduction efficiency of the system. More trials of the photocatalytic reduction experiment should be performed with ZnO-PANI and Ni-ZnO-PANI nanocomposites with a range of nanoparticle sizes to determine the effect of size on the removal percentage. Since most industrial waste water contains a multitude of cations and anions, the effect of some of common anions, such as nitrate, phosphate, and sulfate, on the photocatalytic reduction potential of the photocatalysts should be evaluated. Some anions may adsorb to the PANI or compete with the chromate anion for available electrons. Experiments should also be conducted to determine the reuseability of the photocatalyst and the effect that several reduction cycles has on the Cr(VI) reduction potential.

REFERENCES

[1] EPA, Priority Pollutant List. 2015; https://www.epa.gov/sites/production/files/2015-09/documents/priority-pollutant-list-epa.pdf.

[2] Sheikhmohammadi, A.; Mohseni, S. M.; Khodadadi, R.; Sardar, M.; Abtahi, M.; Mahdavi, S.; Keramati, H.; Dahaghin, Z.; Rezaei, S.; Almasian, M.; Sarkhosh, M.; Faraji, M.; Nazari, S. Application of Graphene Oxide Modified with 8-Hydroxyquinoline for the Adsorption of Cr (VI) from Wastewater: Optimization, Kinetic, Thermodynamic and Equilibrium Studies. *Journal of Molecular Liquids* **2017**, *233*, 75–88.

[3] He, C.; Yang, Z.; Ding, J.; Chen, Y.; Tong, X.; Li, Y. Effective Removal of Cr(VI) from Aqueous Solution by 3-Aminopropyltriethoxysilane-Functionalized Graphene Oxide. *Colloids and Surfaces A: Physicochemical and Engineering Aspects* **2017**, *520*, 448–458.

[4] Vengosh, A.; Coyte, R.; Karr, J.; Harkness, J. S.; Kondash, A. J.; Ruhl, L. S.; Merola, R. B.; Dywer, G. S. Origin of Hexavalent Chromium in Drinking Water Wells from the Piedmont Aquifers of North Carolina. *Environmental Science and Technology Letters* **2016**, *3*, 409–414.

[5] Kulkarni, P.; Deshmukh, P.; Jakhade, A.; Kulkarni, S.; Chikate, R. 1,5 Diphenyl Carbazide Immobilized Cross-Linked Chitosan Films: An Integrated Approach Towards Enhanced Removal of Cr(VI). *Journal of Molecular Liquids* **2017**, *247*, 254–261.

[6] Zhitkovich, A. Chromium in Drinking Water: Sources, Metabolism, and Cancer Risks. *Chemical Research in Toxicology* **2011**, *24*, 1617–1629.

[7] Cheng, Q.; Wang, C.; Doudrick, K.; Chan, C. K. Hexavalent Chromium Removal Using Metal Oxide Photocatalysts. *Applied Catalysis B: Environmental* **2015**, *176-177*, 740–748.

[8] APHA/AWWA/WEF, Standard Methods for the Examination of Water and Wastewater. *Standard Methods* **2012**, 541.

[9] Kalidhasan, S.; Santhana Krishna Kumar, A.; Rajesh, V.; Rajesh, N. The Journey Traversed in the Remediation of Hexavalent Chromium and the Road Ahead Toward Greener Alternatives- A Perspective. *Coordination Chemistry Reviews* **2016**, *317*, 157–166.

[10] Čadková, E.; Chrastný, V. Isotope Evidence of Hexavalent Chromium Stability in Groundwater Samples. *Chemosphere* **2015**, *138*, 74–80.

[11] Jobby, R.; Jha, P.; Yadav, A. K.; Desai, N. Chemosphere Biosorption and Biotransformation of Hexavalent Chromium [Cr(VI)]: A Comprehensive Review. *Chemosphere* **2018**, *207*, 255–266.

[12] Pradhan, D.; Sukla, L. B.; Sawyer, M.; Rahman, P. K. Recent Bioreduction of Hexavalent Chromium in Wastewater Treatment: A Review. *Journal of Industrial and Engineering Chemistry* **2017**, *55*, 1–20.

[13] Kan, C. C.; Sumalinog, M. J. R.; Rivera, K. K. P.; Arazo, R. O.; de Luna, M. D. G. Ultrasound-Assisted Synthesis of Adsorbents from Groundwater Treatment Residuals for Hexavalent Chromium Removal from Aqueous Solutions. *Groundwater for Sustainable Development* **2017**, *5*, 253–260.

[14] Singh, S.; Ahmed, I.; Haldar, K. K. Nickel Oxide Decorated Zinc Oxide Composite Nanorods: Excellent Catalyst for Photoreduction of Hexavalent Chromium. *Journal of Colloid And Interface Science* **2018**, *523*, 1–6.

[15] Wasim, S.; Latif, M.; Bhatti, T. M. Hydrometallurgy Removal of Cr (VI) using Iron Nanoparticles Supported on Porous Cation-Exchange Resin. *Hydrometallurgy* **2015**, *157*, 82–89.

[16] Ahmed, F.; Kumar, S.; Arshi, N.; Anwar, M. S.; Su-Yeon, L.; Kil, G. S.; Park, D. W.; Koo, B. H.; Lee, C. G. Preparation and Characterizations of Polyaniline (PANI)/ZnO Nanocomposites Film using Solution Casting Method. *Thin Solid Films* **2011**, *519*, 8375–8378.

[17] Abdi, S.; Dorranian, D. Effect of CTAB Concentration on the Properties of ZnO Nanoparticles Produced by Laser Ablation Method in CTAB Solution. *Optics and Laser Technology* **2018**, *108*, 372–377.

[18] Nandi, I.; Mitra, P.; Banerjee, P.; Chakrabarti, A.; Ghosh, M.; Chakrabarti, S. Ecotoxicological Impact of Sunlight Assisted Photoreduction of Hexavalent Chromium Present in Wastewater with Zinc Oxide Nanoparticles on Common Anabaena Flos-Aquae. *Ecotoxicology and Environmental Safety* **2012**, *86*, 7–12.

[19] Kumar, S. G.; Rao, K. S. Comparison of Modification Strategies Towards Enhanced Charge Carrier Separation and Photocatalytic Degradation Activity of Metal Oxide Semiconductors (TiO2, WO3 and ZnO). *Applied Surface Science* **2017**, *391*, 124–148.

[20] Jin, Z.; Zhang, Y.-x.; Meng, F.-l.; Jia, Y.; Luo, T.; Yu, X.-y. Facile Synthesis of Porous Single Crystalline ZnO Nanoplates and their Application in Photocatalytic Reduction of Cr(VI) in the Presence of Phenol. *Journal of Hazardous Materials* **2014**, *276*, 400–407.

[21] Zou, T.; Wang, C.; Tan, R.; Song, W.; Cheng, Y. Preparation of Pompon-Like ZnO-PANI Heterostructure and its Applications for the Treatment of Typical Water Pollutants under Visible Light. *Journal of Hazardous Materials* **2017**, *338*, 276–286.

[22] Shouli, B.; Liangyuan, C.; Dianqing, L.; Wensheng, Y.; Pengcheng, Y.; Zhiyong, L. Chemical Different Morphologies of ZnO Nanorods and their Sensing Property. *Sensors & Actuators: B. Chemical* **2010**, *146*, 129–137.

[23] Zhai, H.-j.; Wu, W.-h.; Lu, F.; Wang, H.-s.; Wang, C. Effects of Ammonia and Cetyltrimethylammonium Bromide (CTAB) on Morphologies of ZnO Nano- and Micro-materials under Solvothermal Process. *Materials Chemistry and Physics* **2008**, *112*, 1024–1028.

[24] Yan, X.; Hu, D.; Li, H.; Li, L.; Chong, X.; Wang, Y. Nanostructure and Optical Properties of M Doped ZnO (M Ni , Mn) Thin Films Prepared by SolGel Process. *Physica B: Physics of Condensed Matter* **2011**, *406*, 3956–3962.

[25] Liu, J.; Zhao, Y.; Ma, J.; Dai, Y.; Li, J.; Zhang, J. Flower-Like ZnO Hollow Microspheres on Ceramic Mesh Substrate for Photocatalytic Reduction of Cr(VI) in Tannery Wastewater. *Ceramics International* **2016**, *42*, 15968–15974.

[26] Hasanpoor, M.; Aliofkhazraei, M.; Delavari, H. Microwave-assisted Synthesis of Zinc Oxide Nanoparticles. *Procedia Materials Science* **2015**, *11*, 320–325.

[27] Zhu, P.; Zhang, J.; Wu, Z.; Zhang, Z. Microwave-Assisted Synthesis of Various ZnO Hierarchical Nanostructures: Effects of Heating Parameters of Microwave Oven. *Crystal Growth and Design* **2008**, *8*, 3148–3153.

[28] Liu, X.; Lv, T.; Pan, L.; Sun, Z.; Sun, C. Microwave-Assisted Synthesis of ZnO for Photocatalytic Reduction of Cr(VI) in Aqueous Solution. *Desalination and Water Treatment* **2012**, *42*, 216–221.

[29] Turkyilmaz, S. S.; Guy, N.; Ozacar, M. Photocatalytic Efficiencies of Ni, Mn, Fe and Ag Doped ZnO Nanostructures Synthesized by Hydrothermal Method: The Synergistic/Antagonistic Effect between ZnO and Metals. *Journal of Photochemistry and Photobiology A: Chemistry* **2017**, *341*, 39–50.

[30] Amirthavalli, C.; Manikandan, A.; Prince, A. A. M. Effect of Zinc Precursor Ratio on Mor-

phology and Luminescent Properties of ZnO Nanoparticles Synthesized in CTAB Medium. *Ceramics International* **2018**, *44*, 15290–15297.

[31] Qamar, M.; Gondal, M. A.; Yamani, Z. H. Laser-Induced Efficient Reduction of Cr(VI) Catalyzed by ZnO Nanoparticles. *Journal of Hazardous Materials* **2011**, *187*, 258–263.

[32] Nsib, M. F.; Saafi, S.; Rayes, A.; Moussa, N.; Houas, A. Enhanced Photocatalytic Performance of NiZnO/Polyaniline Composite for the Visible-Light Driven Hydrogen Generation. *Journal of the Energy Institute* **2016**, *89*, 694–703.

[33] Chakrabarti, S. Hexavalent Chromium in Wastewater Using Zinc Oxide Semiconductor Catalyst: A Comparison of Performances Between Micro and Nanoparticles. *Physical Chemical and Biological Treatment Processes* **2015**,

[34] Li, J.; Xiao, Z.; Hu, W.; Zhou, X.; Zheng, X. Improved Photocatalytic Performance of ZnO Prepared by SolGel Method with the Assistance of CTAB. *Materials Letters* **2013**, *91*, 301–303.

[35] Maiti, U. N.; Nandy, S.; Karan, S.; Mallik, B.; Chattopadhyay, K. K. Enhanced Optical and Field Emission Properties of CTAB-Assisted Hydrothermal Grown ZnO Nanorods. *Applied Surface Science* **2008**, *254*, 7266–7271.

[36] Ambalgi, S. M.; Inamdar, H. K.; Manjula, V. T.; Nagaraja, S.; Shrishail, G. Synthesis, Characterization and Electrical Properties of Polyaniline/ Nickel Oxide Synthesis, Characterization and Electrical Properties of Polyaniline/ Nickel Oxide Nanocomposites. *International Journal of Engineering Research* **2016**, *5.2*, 119–122.

[37] Ghotbi, M. Y. Particuology Nickel Doped Zinc Oxide Nanoparticles Produced by Hydrothermal Decomposition of Nickel-Doped Zinc Hydroxide Nitrate. *Particuology* **2012**, *10*, 492–496.

[38] Li, J.; Yan, D.; Hou, S.; Lu, T.; Yao, Y.; Chua, D. H. C.; Pan, L. Metal-Organic Frameworks Derived Yolk-Shell ZnO/ NiO Microspheres as High-Performance Anode Materials for Lithium-Ion Batteries. *Chemical Engineering Journal* **2018**, *335*, 579–589.

[39] Cheng, Polyaniline Hybridized Surface Defective ZnO Nanorods with Long-Term Stable Photoelectrochemical Activity. *Applied Surface Science* **2016**, *383*, 165–176.

[40] Villalba, P.; Ram, M. K.; Gomez, H.; Bhethanabotla, V.; Helms, M. N.; Kumar, A.; Kumar, A. Cellular and in Vitro Toxicity of Nanodiamond-Polyaniline Composites in Mammalian and Bacterial Cell. *Materials Science & Engineering C* **2012**, *32*, 594–598.

[41] Ibarra, L. E.; Tarres, L.; Bongiovanni, S.; Barbero, C. A.; Kogan, M. J.; Rivarola, V. A.; Bertuzzi, M. L.; Yslas, E. I. Ecotoxicology and Environmental Safety Assessment of Polyaniline Nanoparticles Toxicity and Teratogenicity in Aquatic Environment using Rhinella Arenarum Model. *Ecotoxicology and Environmental Safety* **2015**, *114*, 84–92.

[42] Wang, M.; Ji, G.; Zhang, B.; Tang, D.; Yang, Y.; YouweiDu,; Pani, F. O.; Wang, M.; Ji, G.; Zhang, B.; Tang, D.; Yang, Y.; Du, Y. Controlled Synthesis and Microwave Absorption Properties of NiO6-ZnO4-Fe2O4/PANI Composite via an In-Situ Polymerization Process. *Journal of Magnetism and Magnetic Materials* **2015**, *377*, 52–58.

[43] Xu, K.; Liu, C.; Chen, R.; Fang, X.; Wu, X.; Liu, J. Structural and Room Temperature Ferromagnetic Properties of Ni Doped ZnO Nanoparticles via Low-Temperature Hydrothermal Method. *Physica B: Physics of Condensed Matter* **2016**, *502*, 155–159.

[44] Elilarassi, R.; Chandrasekaran, G. Synthesis and Optical Properties of Ni-Doped Zinc Oxide Nanoparticles for Optoelectronic Applications. *Optoelectronics Letters* **2010**, *6*.

[45] Gunti, S.; Alamro, T.; McCrory, M.; Ram, M. K. The Use of Conducting Polymer to Stabilize the Nanostructured Photocatalyst for Water Remediation. *Journal of Environmental Chemical Engineering* **2017**, *5*, 5547–5555.

[46] Ibrahim, K. A. Synthesis and Characterization of Polyaniline and Poly(aniline-co-o-nitroaniline) using Vibrational Spectroscopy. *Arabian Journal of Chemistry* **2017**, *10*, S2668–S2674.

[47] Sharma, S.; Singh, S.; Khare, N. Enhanced Photosensitization of Zinc Oxide Nanorods using Polyaniline for Efficient Photocatalytic and Photoelectrochemical Water Splitting. *International Journal of Hydrogen Energy* **2016**, *41*, 21088–21098.

[48] EPA, U. *Method 7196A Hexavalent Chromium (Colorimetric)*; 1992; pp 1–6.

[49] Pflaum, R. T.; Howi, L. C. The Chromium-Diphenylcarbazide Reaction. **1956**, *78*, 4862–4866.

[50] Sharma, B. K.; Gupta, A. K.; Khare, N.; Dhawan, S. K.; Gupta, H. C. Synthesis and Characterization of Polyaniline ZnO Composite and its Dielectric Behavior. *Synthetic Metals* **2009**, *159*, 391–395.

[51] Bhaumik, M.; Kumar, V.; Maity, A. Journal of Environmental Chemical Engineering Synergetic Enhancement of Cr(VI) Removal from Aqueous Solutions using Polyaniline- Ni(OH)2 Nanocomposites Adsorbent. *Journal of Environmental Chemical Engineering* **2018**, *6*, 2514–2527.

[52] Naimi-joubani, M.; Shirzad-siboni, M.; Yang, J.-k.; Gholami, M. Photocatalytic Reduction of Hexavalent Chromium with Illuminated ZnO/ TiO2 Composite. *Journal of Industrial and Engineering Chemistry* **2015**, *22*, 317–323.

[53] Shirzad-siboni, M.; Farrokhi, M.; Darvishi, R.; Soltani, C.; Khataee, A. Photocatalytic Reduction of Hexavalent Chromium over ZnO Nanorods Immobilized on Kaolin. **2014**,

[54] Assadi, A.; Dehghani, M. H.; Rastkari, N.; Nasseri, S.; Mahvi, A. H. Photocatalytic Re-

duction of Hexavalent Chromium in Aqueous Solutions with Zinc Oxide Nanoparticles and Hydrogen Peroxide. *Environmental Protection Engineering* **2012**, *38*.

[55] Guzman, F.; Chuang, S. S. C.; Yang, C. Role of Methanol Sacrificing Reagent in the Photocatalytic Evolution of Hydrogen. *Industrial and Engineering Chemistry Research* **2013**, *52*, 61–65.

[56] Chenthamarakshan, C. R.; Yang, H.; Ming, Y.; Rajeshwar, K. Photocatalytic Reactivity of Zinc and Cadmium Ions in UV-Irradiated Titania Suspensions. *Journal of Electroanalytical Chemistry* **2000**, *494*, 79–86.

[57] Tan, T.; Beydoun, D.; Amal, R. Effects of Organic Hole Scavengers on the Photocatalytic Reduction of Selenium Anions. *Journal of Photochemistry and Photobiology A* **2003**, *159*, 273–280.